Supporting Information

Grishchuk *et al.* 10.1073/pnas.0807859105

SI Text

Part 1. The Laser Trap and Other Devices. Our instrument is based on the Zeiss Axiophot2 microscope and incorporates lasers for trapping, position detection, alignment, fluorescence excitation and photobleaching. The microscope and laser optics are attached to an optical air table (Melles Griot, model 07 OFA) inside a temperature-controlled room (±0.5°C). A shelf above the microscope holds the power blocks for a Zeiss HBO 100W lamp and various control devices. A Plexiglas box surrounds the laser optics to suppress convection currents. The microscope body was extensively modified to improve its mechanical stability and to accommodate five lasers without diminishing its imaging capabilities. The microscope's objective turret was replaced with a custom mount attached to the breadboard and supported from the optical table by two strong aluminum stands; this helps to minimize vibrations from the moving parts of the turret. A microscope stage (Ludl Electronic Products, model 99S000) is manually controlled with a joystick for sample scanning. Mounted on this stage is a three-axis piezo-electric stage (Physik Instrumente, model P-527.3CL), which is used to digitally control the specimen's position in increments of 1.0 nm over a 100 × 100 × 20 μm volume. Coarse focusing is accomplished with a nonmotorized focus knob. To minimize downward stage drift, the stage is additionally supported by two springs of adjustable stiffness that compensate for its weight. The microscope condenser was custom built to allow its penetration through the narrow opening in the piezo-stage, but it contains the lenses, polarizer, and Wollaston prism from a Zeiss oil-immersion condenser. For laser trapping and DIC, we used a 1.3-NA Plan-Neofluar 100X objective (Zeiss Inc.). Fluorescent imaging was carried out with 1.4x NA objective (α Plan-Fluar 100X, Zeiss Inc.).

A 488-nm Argon ion laser (Melles Griot, series 532, model 35 LAS 450, 488 nm) and a 532-nm diode laser (Beta Electronics, model MGM100, 532 nm) were used for fluorescence excitation and photobleaching (Fig. S4). Their optical paths are elevated from the optical table, so they can be optically connected with the epi-illumination path. The optical trapping and detection components are similar to those described in refs. 1 and 2. An acousto-optical deflector (IntraAction Corp., model DTD-406BB6) was used for computer steering of the trapping laser beam (Spectra-Physics Lasers, model J20-BL10-106Q, 1064 nm). A detection laser (Blue Sky Research, model FTEC0852-075SFP) provides a 855-nm beam for tracking a trapped bead. A Gelium-Neon 630-nm laser (Melles Griot, model 25 LHR 991-249) was used to facilitate the alignment of the trapping and detection lasers. The trap and detector beams enter the microscope's imaging path below the fluorescence filter cubes, so the cubes can be changed without affecting the intensity or other properties of the beams. These laser beams are directed into the objective by a dichroic mirror (Omega, 730DCSPXR), which allows ≈90% transmission of the microscope light from 380 to 700 nm. Signals from the four elements of a quadrant photodetector (QPD, custom built, based on a design by T. Perkins, Boulder CO) are preamplified and passed through a differential amplifier (frequency range 0–100 kHz). This supplies normalized x- and y-position signals and a third signal, which represents the average intensity on all four QPD quadrants before digitization by a 16-bit A/D board (National Instruments, PCI-6070E).

Two-dimensional calibrations were carried out as in ref. 3. The cross-talk between x- and y-position signals was <5%. In all our experiments, the QPD was sampled at 4 kHz without additional filtering or processing; the smallest detectable bead displacement was ≈3 nm; the smallest force measured was ≈0.03 pN; free bead relaxation time was <20 ms. At the end of each useful experiment, the QPD and trap stiffness were calibrated with the same bead by using the equipartition method (4). Programs for calibration and instrument control were written in LabVIEW 6i (National Instruments). Specimen temperature was regulated to 32.0 ± 0.5°C by electronically controlled heaters on the condenser (custom made) and objective lenses (Bioptechs).

Part 2. Mathematical Modeling and Data Analysis.

Data analysis. All numbers in figures are means ± SEMs, unless stated otherwise. MT disassembly rates in the absence of Dam1 were determined by DIC microscopy under the same conditions as in experiments with Alexa488-Dam1. Five measurements of >80 μm/min in Dam1's absence and two such measurements in the presence of Dam1–19 are not shown in Fig. 3*A* to reduce figure size, but these values were included in the analyses. Spectral characteristics of bead's tracings were analyzed with MatLab6.5 software.

Mathematical modeling. An MT and interacting ring were modeled and analyzed as described in ref. 5 with modifications. A 0.5-μm bead is assumed to attach strongly to a single, ring-associated Dam1 heterodecamer. Attachment to two heterodecamers does not change model conclusions. The binding is assumed to be rigid, so the bead's center is always positioned on a line that contains the center of this subunit and the ring. When the ring tilts, the bead may come in contact with the MT wall or with bending PFs. To take this into account, the total energy of the system (Eq. 8 in *SI Text* in ref. 5) has additional terms. These describe the bead's repulsion from tubulins upstream and downstream from the bead, when the distances between centers of the bead and tubulin monomers are less than the sum of their radii. All other model parameters are the same as in ref. 5: A = 28 k_BT, B = 300 k_BT /Rad, χ_o = 0.2 Rad, r_o = 0.8 Å, r_{DAM} = 1.4 Å, k_{spring} = 0.13 N/m, k_{flex} = 20 k_BT /Rad; unless stated otherwise k_{DAM} = 13 k_BT.

Model results: Ring's wobbling is highly stochastic. A ring moving under the depolymerization force will change its orientation, as ring's linkers search for the minimum-energy configurations of their bonding with helical MT lattice. The positions of tubulin in the MT wall and thus the sites of preferred ring binding are periodic. In the absence of thermal fluctuations, the ring's tilting angles should also be periodic, and the spectrum should show a few discrete frequencies, each of which would correspond to the times for specific ring transitions between the most preferred configurations on MT lattice. The amplitudes for these frequencies would reflect the probability of each corresponding transition. However, the stochasticity of ring movement and thermal fluctuations blur these discrete peaks, so in our calculations they appear with different amplitudes for different ring–MT pairs. The pattern of frequency distributions is expected to be even more disordered for a ring-attached bead, because the bead's oscillations do not mirror those of the ring exactly.

Comparison of theoretical and experimental results: Coupling to the bead in the absence of load does not change significantly the ring's tracking. We have analyzed our model's predictions for the behavior of a bead–ring complex, because these predictions can be tested experimentally. The MT-driven ring movements are relatively slow (the measured MT-driven motion of the ring was >100-times slower than the measured bead relaxation time, which was <0.5 ms). Therefore, in aqueous solution and without an applied

load, the bead's thermal motion should not impede ring movements. Indeed, in our model, movements of the center of a ring that is bound to a bead are highly similar to the movements of the same ring without an attached bead (Fig. 4*B*). This corresponds well with our experimental result that the rate of Dam1 tracking at the end of a depolymerizing MT and the rate of bead movement in the presence of soluble Dam1 were similar (5.4 ± 0.5 μm/min vs. 7.9 ± 1.0 μm/min, see this work and ref 6).

Comparison of our results with published data. Previous studies have suggested that a Dam1 ring allows MTs to generate pulling force in the 0.5- to 3-pN range (7). These studies have used Dam1-coated beads that are prepared highly similarly to ours, but they were done in the absence of soluble Dam1 complexes. Based on this and other facts, such as the absence of strong reducing agents in ref. 7, we have previously suggested that these beads were coupled to the MT tips in the absence of the MT-encircling rings. We have also provided several arguments that indicate that in our assays in the presence of soluble Dam1 the beads are attached to the encircling Dam1 complexes (this work and ref. 6). The maximum force measured in our experiments with these beads was ≈5 pN (average 2.4 pN). It seems surprising that this value is not much higher than the value reported in ref. 7. However, measurements of the forces transduced by the couplers with different geometries in our system are internally consistent. Forces measured with streptavidin-coated beads, which attach laterally to the MT wall, are approximately sixfold smaller than with Dam1 rings, just as one would predict. We also studied Dam1-coated beads associating with MTs in the absence of soluble Dam1, conditions where rings do not form. In our system, however, these beads fail to bind strongly enough to the GDP-segments of MTs for us to make a measurement, even when the beads were held against the MT wall with the laser trap. This implies that the force such beads can experience from depolymerizing MTs before detaching is too small for us to measure. Thus, in our system, with a small number of Dam1-MT bonds, the forces are 10 times smaller than when Dam1 rings can form.

In our assays the Dam1 forces are almost certainly subjected to a torque. This is unlike a description of a system in which the bead was allowed to attach to the end of a growing MT (7). Specifically, we suggest that the average force of 2.4 pN with which our trap can cause stalling/detachment of the Dam1-ring-associated bead balances ≈30 pN from the MT depolymerization force. This interpretation is strongly supported by our reporting here that in our system the smaller streptavidin-coated beads are stalled by larger trapping forces (Fig. 1*E*). We therefore think that the evidence for the validity of our mechanical interpretations for this system is significant. However, we have no definitive answer to the question of what is being measured in ref. 7. Our experimental systems, reagents, and conditions are quite different from this published study. The forces that they suggest are experienced by the Dam1 complexes under MT depolymerization are in fact the same forces that allowed processive bead motions toward the growing PLUS MT end. In this system, there seems to be a significant possibility that the measurement is reporting the affinity, i.e. force required to detach a Dam1-coated bead from the MT end, not a force developed by MT depolymerization. The mechanics of this system has not yet been investigated, and there have been no systematic comparisons under these conditions of different bead sizes and of the encircling vs. nonencircling complexes. Development of the corresponding model would also be helpful in reconciling the results obtained in different experimental systems and under different conditions.

It is noteworthy that in the absence of soluble Dam1, the Dam1-coated beads bound well to the guanosine-5′-[(α,β))-methyleno]triphosphate (GMPCPP) tips of our segmented MTs, and when the caps were removed with laser bleaching, approximately half of the beads moved with the shortening GDP-containing segments by rolling on MT surface (6). It is interesting that the beads that show no persistent binding to the GDP-tubulin lattice would move persistently, remaining attached over long distances. We think that the bead's attachment at a shortening MT end is stabilized by its rolling and the fact that the shortening PFs are curled. In a straight segment of MT wall, a bead can bind to only a few dimers, but with the curling PF, the number of bonds should increase, so the bead is attached more strongly, and can move by rolling. This mode of motion seems a poor model for chromosome motility, so we did not pursue its analysis.

1. Visscher K, Block SM (1998) Versatile optical traps with feedback control. *Methods Enzymol* 298:460–489.
2. Brouhard GJ, Schek HT, III, Hunt AJ (2003) Advanced optical tweezers for the study of cellular and molecular biomechanics. *IEEE Trans Biomed Eng* 50:121–125.
3. Lang MJ, Asbury CL, Shaevitz JW, Block SM (2002) An automated two-dimensional optical force clamp for single molecule studies. *Biophys J* 83:491–501.
4. Sheetz MP, ed (1998) *Laser tweezers in Cell Biology* (Academic Press, San Diego).
5. Efremov A, Grishchuk EL, McIntosh JR, Ataullakhanov FI (2007) In search of an optimal ring to couple microtubule depolymerization to processive chromosome motions. *Proc Natl Acad Sci USA* 104:19017–19022.
6. Grishchuk EL, *et al*. (2008) Different assemblies of the DAM1 complex follow shortening microtubules by distinct mechanisms. *Proc Natl Acad Sci USA* 105:6918–6923.
7. Asbury CL, Gestaut DR, Powers AF, Franck AD, Davis TN (2006) The Dam1 kinetochore complex harnesses microtubule dynamics to produce force and movement. *Proc Natl Acad Sci USA* 103:9873–9878.
8. Franck AD, Powers AF, Gestaut DR, Gonen T, Davis TN, Asbury CL (2007) Tension applied through the Dam1 complex promotes microtubule elongation providing a direct mechanism for length control in mitosis. *Nat Cell Biol* 9:832–837.
9. Grishchuk EL, Molodtsov MI, Ataullakhanov FI, McIntosh JR (2005) Force production by disassembling microtubules. *Nature* 438:384–388.

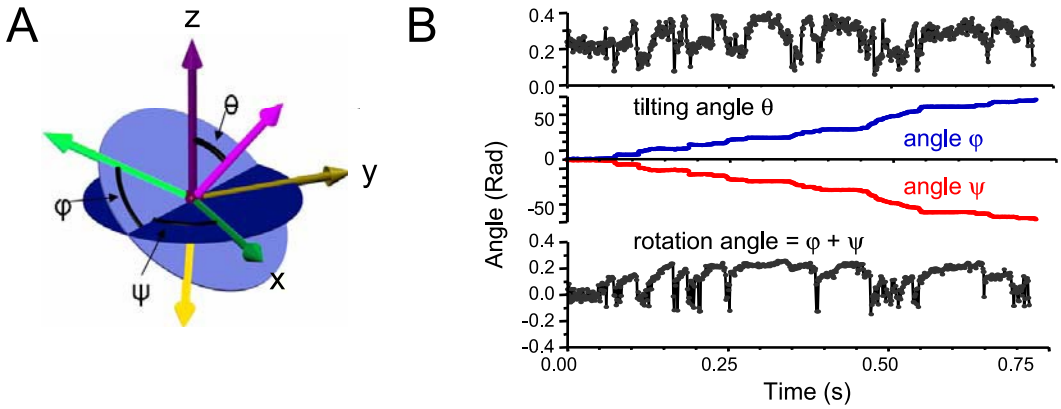

Fig. S1. Wobbling of a theoretical ring. (*A*) Angular variables of ring orientation (see Suppl. ref. 5 for details). Axis *z* is along the MT axis, pointing toward the plus end. (*B*) Model results that demonstrate wobbling of the ring as it moves under the force of a depolymerizing MT (k_{DAM} = 13 k_BT). The angle between the ring's normal and the MT axis oscillates from 5° to 25°, but the ring is almost always tilted (angle θ is 0 when the ring's plane is perpendicular to MT). Angles φ and ψ, which define the orientation of the ring relative to the MT seam, change monotonically and in concert, but their average sum, the rotation angle, does not change significantly. This means that although the ring's axis undergoes precession (it describes a cone around the MT axis), rotation of the ring is virtually absent ($<$ 20°). Compared with the angular separation between PFs (360/13 $\approx$ 28°), this is modest. Therefore, the linkers between an MT and a theoretical ring coupler walk along their corresponding PFs (Suppl. ref. 5). This result fits well with a behavior of a real Dam1 ring, as visualized via an attached bead: when moving at the shortening MTs, beads show no significant rotations around the MT (Suppl. ref. 6).

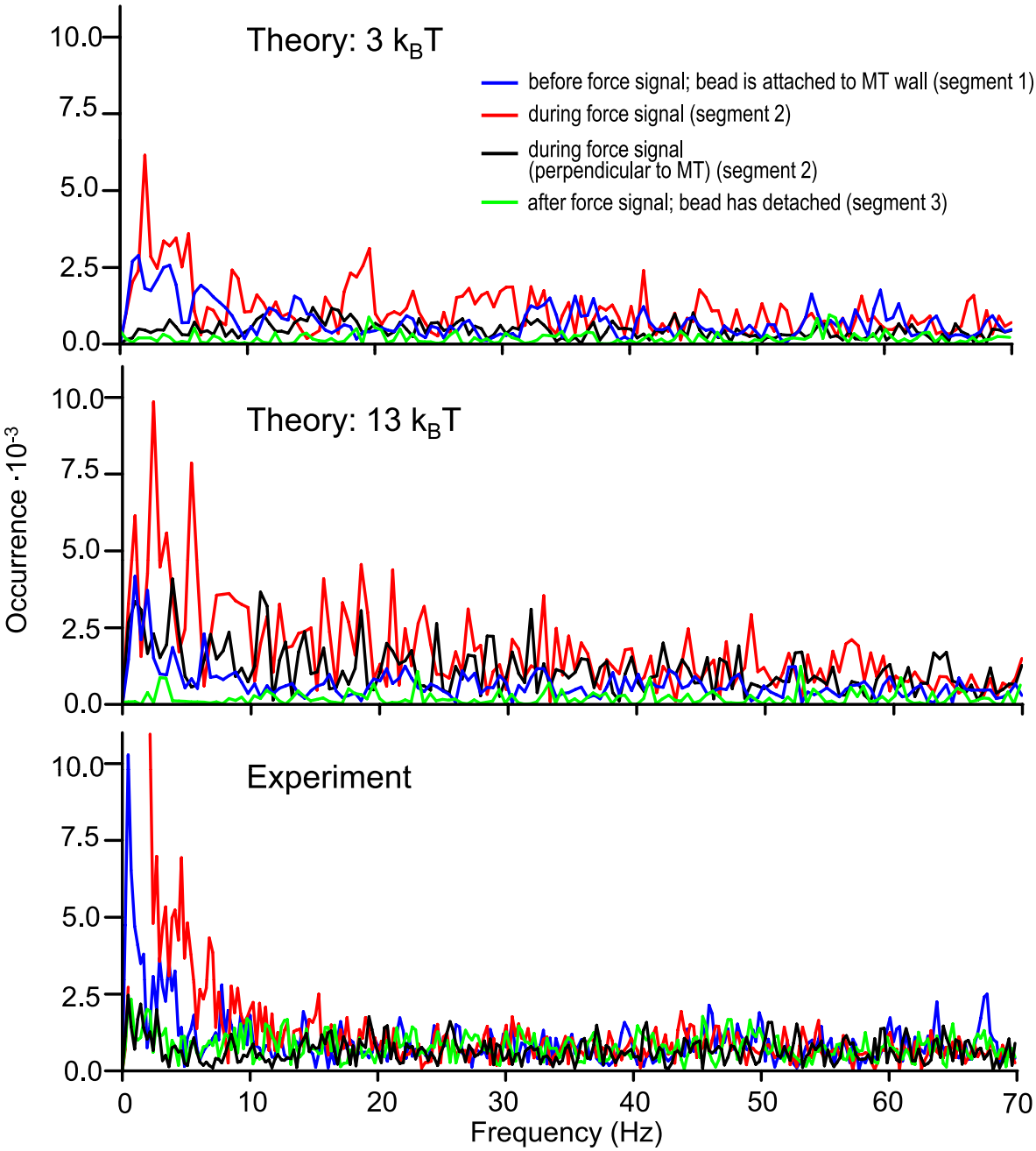

Fig. S2. Irregular oscillations of ring-associated beads as predicted by theory and seen in experiment. These theoretical spectra are the same as in Fig. 4*C*, but shown for up to 70 Hz. The traces are for bead motions parallel to the MT axis, unless stated otherwise. Segments of beads tracings were chosen for analysis as illustrated in Fig. 4*E*. Although there is considerable variability in the positions of peaks in the tracings parallel to the MT during beads MT-depolymerization-induced motions (in red), peak values for weaker bonds rarely exceed 4×10^{-3}. Both theoretical and experimental spectra occasionally revealed bead oscillations parallel to the MT before MT depolymerization (blue traces). The stochasticity of the MT–ring–bead system prohibits accurate quantitative comparison of the theoretical predictions and experimental data set, but the overall features of these spectra are similar, while the heights of the peaks in experimental data are reminiscent of the peaks in spectra from stronger binding theoretical rings.

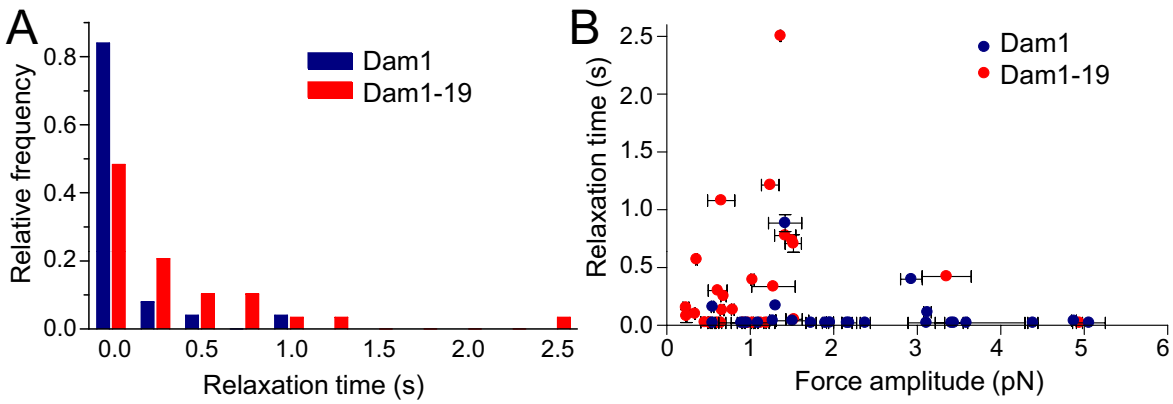

Fig. S3. Analysis of the descending parts of the force signals. When MT depolymerization reaches the site of the bead's attachment, the bead begins to move toward the MT minus end (and away from the trap's center), but a majority of the beads fail to escape from the trap and ultimately fall back to its center. This reverse motion is seen as a descending part of the force signal. It can be characterized with a ''relaxation time,'' the approximate duration of the reverse motion (see Suppl. ref. 9 for details). (*A*) Histogram distribution for the relaxation times seen in experiments with different Dam1 proteins. With wild-type complexes, the bead usually jumps to the center of the trap abruptly, as if the ring slipped of the MT end or lost its attachment to the bead. With the Dam1–19 mutant, longer relaxation times are more common. They are usually seen in signals with smaller force amplitudes (*B*), similar to a behavior of the beads attached to MTs with nonencircling couplers (Suppl. ref. 9). This observation suggests that some of these beads were attached to the nonencircling patches of Dam1–19, rather than full rings. These ringless oligomers could have contributed to the fast rate of MT-end tracking of Dam1–19 complexes (Fig. 3*F*). Future work should focus on quantitative characterization of the ring formation by Dam1–19 oligomers, so that the contribution from the nonencircling forms of Dam1–19 can be taken into account.

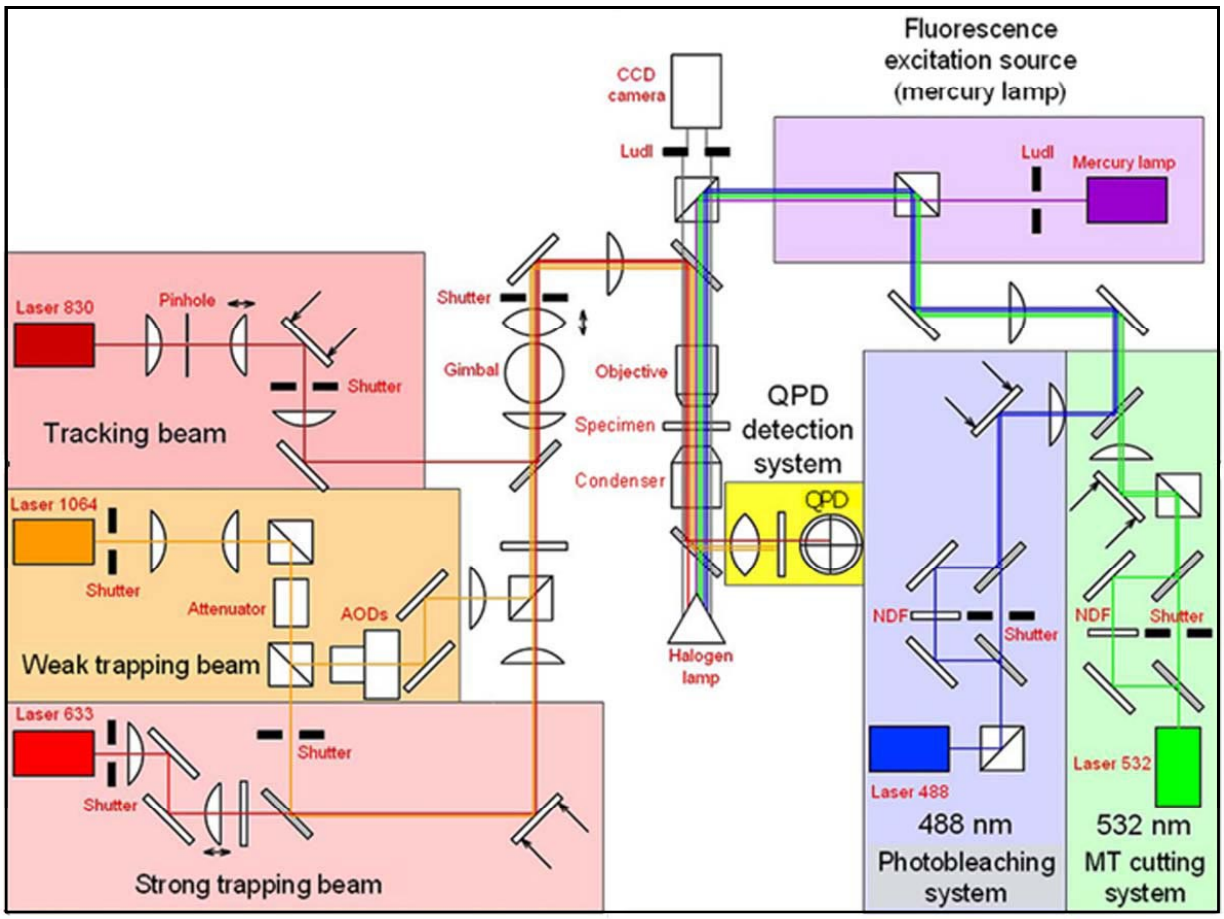

Fig. S4. Diagram of our microscope system. See *SI Text*.

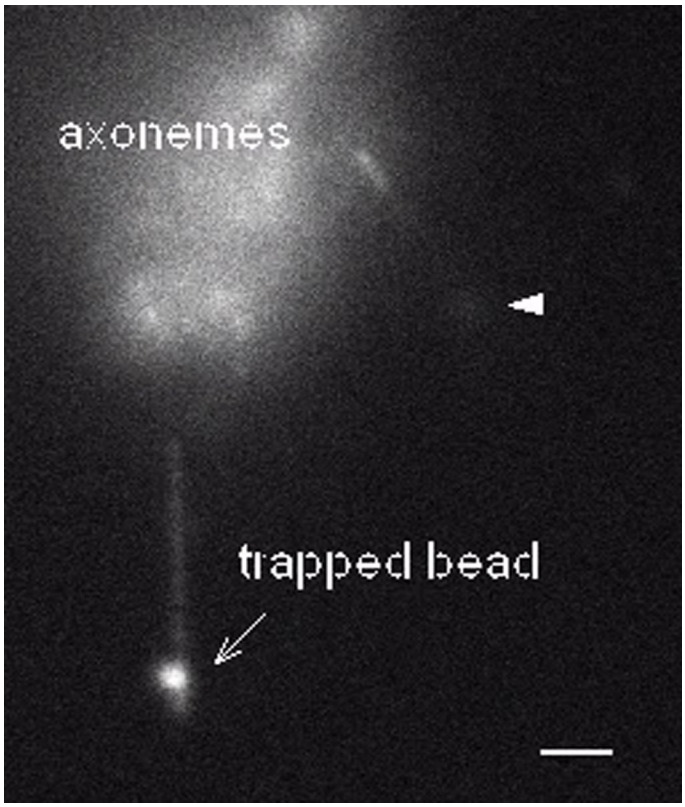

Movie S1. Force measurement with wild type Dam1. Dam1-coated beads were allowed to bind to capped MTs preequilibrated with soluble Dam1. The initial image was acquired with a GFP filter and shows a fluorescent bead (arrow) attached to a MT decorated with Dam1 dots. Subsequent images were taken every second with low-light DIC through a Texas Red filter. A bright green light was turned on to disperse the MT cap 13 s after the start of the experiment. The trapped bead shows virtually no motion, except a tiny jerk (arrows) toward the cluster of axonemes. An untrapped bead (arrowhead) becomes visible as it moves toward the axonemes at 6 μm/min. Both the axonemes and this bead move rapidly at the end of the video because of stage shifts (arrowheads on Fig. 4*E*). The trapped bead does not move, which verifies its complete separation from the MT. (Scale bar, 2 μm.)

Movie S1 (MOV)

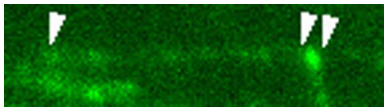

Movie S2. Diffusion of the mutant Dam1–19 complexes. MTs were elongated from coverslip-attached seeds (double arrowheads) and were stabilized by capping their plus ends with rhodaminated GMPCPP tubulin (single arrowhead). After washing away the nucleotides and soluble tubulin, Alexa488-labeled Dam1–19 was allowed to bind the MTs. Green images were acquired continuously with 250-ms exposures by using the GFP filter (played three times faster). Some images were acquired through the Texas Red filter; they confirm that the dots move over the GDP portion of this MT. The MT projects freely in the solution, as is evident from its arc-like thermal motions. A kymograph for this sequence is shown in Fig. 3*C*.

Movie S2 (MOV)

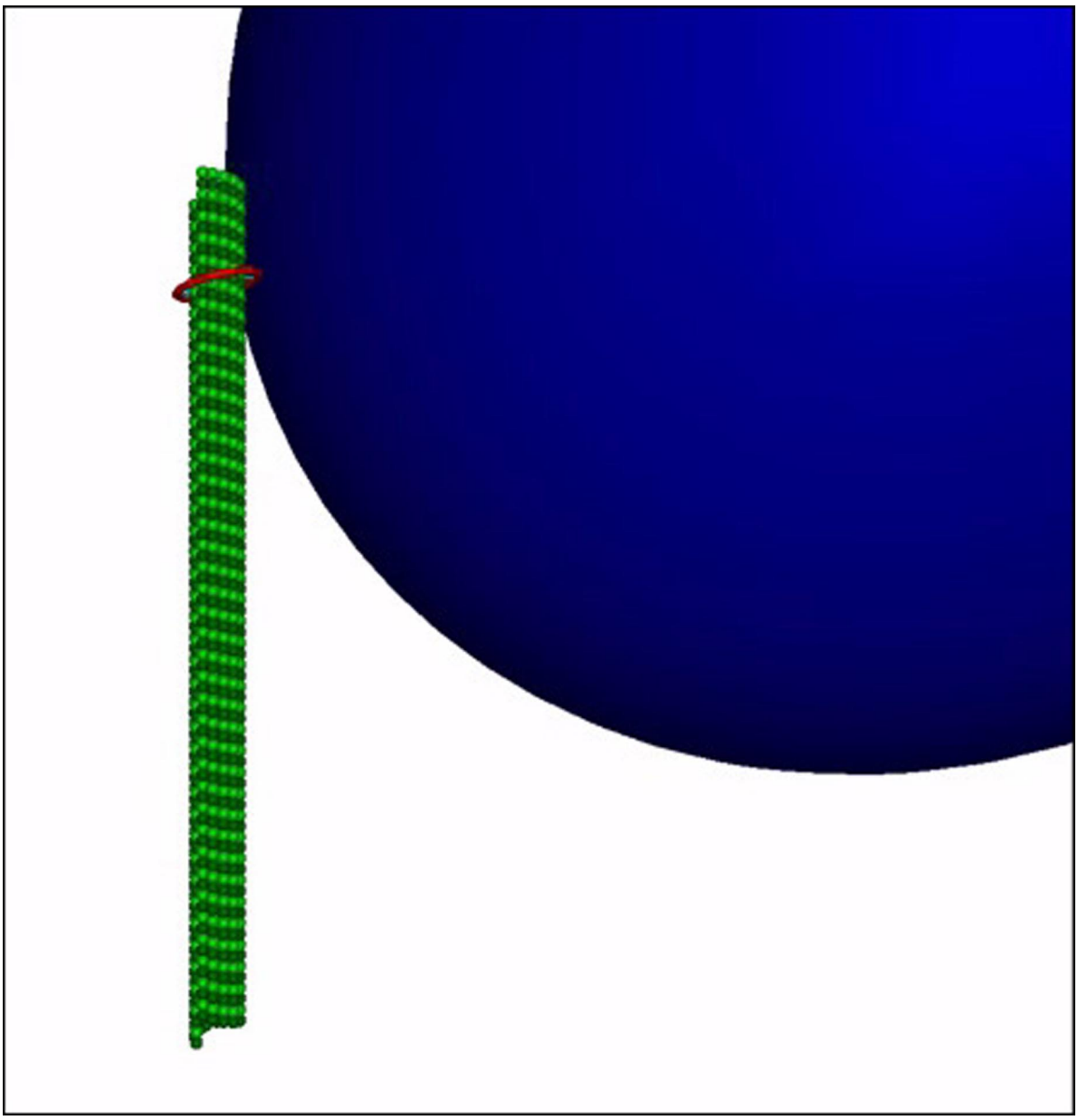

Movie S3. Wobbling of the theoretical ring and its associated bead. Video shows calculated configurations for a Dam1 ring attached to a bead (Dam1-tubulin energy 13k_BT). The ring is bound to an MT with 13 protofilaments whose subunits make a three-start, left-handed helix, the most common MT structure *in vivo*. When the MT depolymerizes, the ring begins to move at 4.6 μm/min. The plane of the moving ring changes its orientation repeatedly without ring rotation around the MT (Fig. S1). This "wobbling" is largely stochastic, but certain orientations are repeated with different frequencies. This video also illustrates the MT-stabilizing properties of the ring coupler. When a ring's motion stalls, PF bending cannot pass the ring, even though the segment of the MT wall immediately under the ring shows some ''breathing''. In an analogous situation, but with a nonencircling coupler, the PFs that are not associated with the coupler would have continued their disassembly, thereby degrading the stability of the cargo's attachment. Model parameters were as described in *SI Text* Part 2. Video is played 100$\times$ slower than "real" time.

Movie S3 (MOV)